AD-A074 471 AIR FORCE GEOPHYSICS LAB HANSCOM AFB MA F/G 4/1
AN ATMOSPHERIC TEMPERATURE PROFILE MEASURED WITH AN IN-SITU INF--ETC(U)
MAY 79 R A MCCLATCHEY, A D D'AGATI
UNCLASSIFIED AFGL-TR-79-0100 NL

| OF |
AD A074471

END
DATE FILMED
10-79
DDC

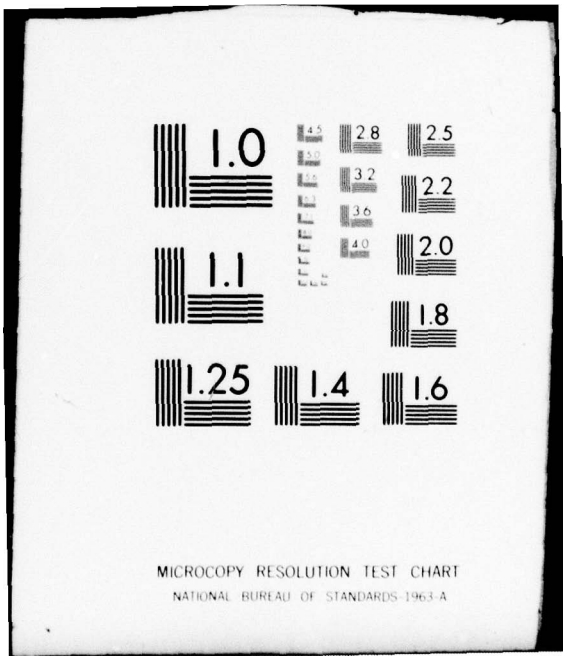
1.0
1.1
1.25
1.4
1.6
1.8
2.0
2.2
2.5
2.8
3.2
3.6
4.0
MICROCOPY RESOLUTION TEST CHART
NATIONAL BUREAU OF STANDARDS-1963-A

AD A074471

(14) AFGL-TR-79-0100, AFGL-ERP-
(9) ENVIRONMENTAL RESEARCH PAPERS, No. 681

(12)

# An Atmospheric Temperature Profile Measured With an In-Situ Infrared Radiometer.

LEVEL II

(10) A. McCLATCHEY
T. D'AGATI

(12) 30p.

(11) 3 May 1979





(16) (17) 13

OPTICAL PHYSICS DIVISION PROJECT 7670
AIR FORCE GEOPHYSICS LABORATORY
HANSCOM AFB, MASSACHUSETTS 01731

AIR FORCE SYSTEMS COMMAND, USAF



409578

This report has been reviewed by the ESD Information Office (OI) and is releasable to the National Technical Information Service (NTIS).

This technical report has been reviewed and is approved for publication.

FOR THE COMMANDER

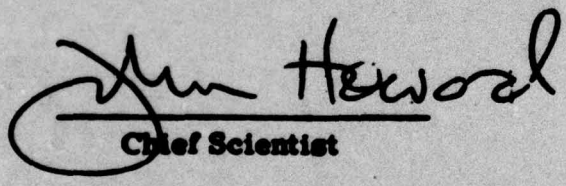

Chief Scientist

Qualified requestors may obtain additional copies from the Defense Documentation Center. All others should apply to the National Technical Information Service.

Unclassified

SECURITY CLASSIFICATION OF THIS PAGE (When Data Entered)

| REPORT DOCUMENTATION PAGE | | READ INSTRUCTIONS BEFORE COMPLETING FORM |
|---|---|---|
| 1. REPORT NUMBER<br>AFGL-TR-79-0100 | 2. GOVT ACCESSION NO. | 3. RECIPIENT'S CATALOG NUMBER |
| 4. TITLE (and Subtitle)<br>AN ATMOSPHERIC TEMPERATURE PROFILE MEASURED WITH AN IN-SITU INFRARED RADIOMETER | | 5. TYPE OF REPORT & PERIOD COVERED<br>Scientific. Interim.<br>6. PERFORMING ORG. REPORT NUMBER<br>ERP No. 661 |
| 7. AUTHOR(s)<br>R. A. McClatchey<br>A. P. D'Agati | | 8. CONTRACT OR GRANT NUMBER(s) |
| 9. PERFORMING ORGANIZATION NAME AND ADDRESS<br>Air Force Geophysics Laboratory (OPI)<br>Hanscom AFB<br>Massachusetts 01731 | | 10. PROGRAM ELEMENT, PROJECT, TASK AREA & WORK UNIT NUMBERS<br>62101F<br>76701304 |
| 11. CONTROLLING OFFICE NAME AND ADDRESS<br>Air Force Geophysics Laboratory (OPI)<br>Hanscom AFB<br>Massachusetts 01731 | | 12. REPORT DATE<br>3 May 1979<br>13. NUMBER OF PAGES<br>29 |
| 14. MONITORING AGENCY NAME & ADDRESS(if different from Controlling Office) | | 15. SECURITY CLASS. (of this report)<br>Unclassified<br>15a. DECLASSIFICATION/DOWNGRADING SCHEDULE |

16. DISTRIBUTION STATEMENT (of this Report)

Approved for public release; distribution unlimited.

17. DISTRIBUTION STATEMENT (of the abstract entered in Block 20, if different from Report)

18. SUPPLEMENTARY NOTES

19. KEY WORDS (Continue on reverse side if necessary and identify by block number)

Remote sounding
Atmospheric transmission
Atmospheric radiation

micrometers

20. ABSTRACT (Continue on reverse side if necessary and identify by block number)

A side-looking infrared radiometer operating in a narrow spectral interval in the 15 $\mu$m carbon dioxide band was flown on a balloon platform. Data were obtained over the altitude range from 9.4 to 30 km. The resulting radiance measurements are compared with calculations making use of independent rawinsonde measurements obtained during the balloon flight. These comparisons indicate a systematic discrepancy of a few percent at lower altitudes increasing to 20 percent near 20 km. This discrepancy is found to be consistent with a

Cont'

DD FORM 1 JAN 73 1473 EDITION OF 1 NOV 65 IS OBSOLETE

Unclassified

SECURITY CLASSIFICATION OF THIS PAGE (When Data Entered)

20. Abstract (Continued)

CONT

previous study of satellite based radiances. Possible sources of this discrepancy are investigated and rejected, leading the authors to question the assumption that the source function is equal to the Planck intensity.

## Preface

We wish to acknowledge the help of the U. S. Army Atmospheric Sciences Laboratory for making available to this program two filter radiometers previously developed under Army support. We further wish to acknowledge the efforts of Dr. David G. Murcray and his group at the University of Denver for their efforts in preparing the radiometers for flight and conducting the balloon flight on 28 September 1977. We are particularly indebted to Mr. Frank H. Murcray for his efforts to carefully perform the sensor calibration prior to flight and to re-examine his calibration procedures after the flight to assess calibration uncertainties. Helpful discussions with Dr. J. I. F. King during the preparation of the manuscript are also gratefully acknowledged.

## Contents



## Illustrations

## Illustrations



## Tables

# An Atmospheric Temperature Profile Measured With an In-Situ Infrared Radiometer

## 1. INTRODUCTION

A great deal of effort has been expended during the past 15 years to develop hardware and analysis techniques to derive vertical distributions of atmospheric temperatures from radiance measurements made from a satellite-based sensor. Most of these measurements have made use of the 15 $\mu$m carbon dioxide band as first suggested by Kaplan[1] and have been based on the fact that carbon dioxide can be taken as uniformly mixed in the free atmosphere. This assumption allows us to make a rather good estimate of the transmission properties of the atmosphere in the spectral region of interest. In principle, then, the radiances, as measured in different spectral intervals of the 15 $\mu$m carbon dioxide band, ranging from the band center to one of the band wings, can be interpreted in terms of the vertical distribution of atmospheric temperature. Figure 1 indicates the basic concept calculated for the U.S. Standard Atmosphere, 1976,[2] in terms of the spectral channels that compose the temperature sounder on the Defense Meteorological Satellite.

---

(Received for publication 1 May 1979)

1. Kaplan, L.D. (1959) Inference of atmospheric structure from remote radiation measurements, J. Op. Soc. Amer. 49:1004.

2. U.S. Standard Atmosphere (1976) NOAA-S/T 76-1562, Supt. of Documents, U.S. Government Printing Office.

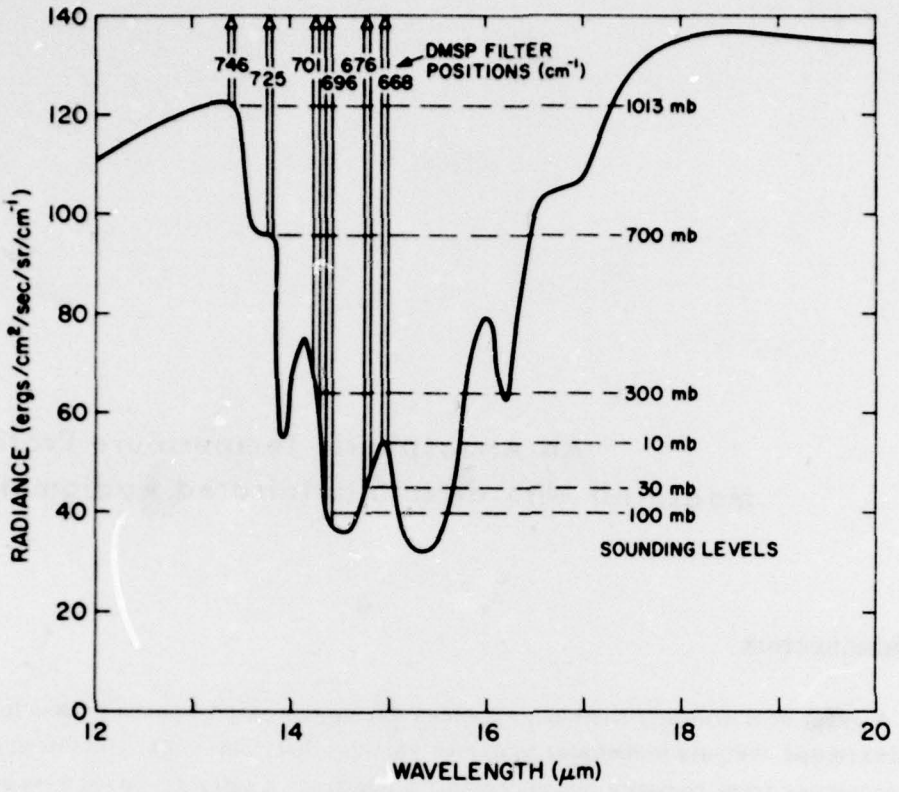


Figure 1. Calculated Spectral Distribution of Upwelling Radiance in the 15 $\mu$m Carbon Dioxide Band. Indicated pressure levels show the portion of the atmosphere responsible for the maximum upwelling emission to space at the frequencies of the DMSP filters

Since the concept of remote temperature sounding of the atmosphere was first suggested, the development of objective inversion algorithms has been fraught with difficulty and largely discarded in favor of statistical techniques requiring climatological data as a basis of comparison. In an effort to get at the root of this difficulty, a project was designed to investigate and verify our ability to solve the "forward problem" that is, the calculation of the expected spectral radiances emerging from an atmosphere whose profile of temperature and moisture is known from radiosonde/rocketsonde measurements.

The Defense Meteorological Satellite Program (DMSP) includes a sensor capable of measuring radiances in the 15 $\mu$m region at frequencies located as indicated in Figure 1. Using several sets of measurements from the DMSP satellite, a

a study of the "forward problem" was conducted by McClatchey.[3] This study began with the identification of a number of satellite measurements made in geographical regions in close proximity in time and space to rawinsonde/rocketsonde stations. Further, an effort was made by inspection of visual and infrared imagery obtained by sensors on the same satellite, to establish that the atmospheric path from surface to satellite was free of clouds. Carbon dioxide was assumed uniformly mixed and the rawinsonde/rocketsonde temperature data were used to compute the upwelling radiation corresponding to the six filter channels of the satellite sensor. With the exception of one channel located near the carbon dioxide band center, all channels for all cases studied showed a significant systematic discrepancy, the calculated values being larger than those measured. The magnitude of this discrepancy is largest in the 707 $cm^{-1}$ channel (15 percent) and smallest in the Q-branch channel centered at 668 $cm^{-1}$.

Three potential sources of these radiance discrepancies have been considered: 1) A sensor calibration error; 2) An uncertainty in the calculated transmittances; and 3) Rawinsonde/rocketsonde temperature errors (or some difference between the rawinsonde temperatures and a radiatively derived temperature). The question of instrument calibration has been investigated and potential uncertainties due to this cause are felt to be far less than those observed. The transmission uncertainty issue is being investigated, and current estimates are that it, too, is unlikely to be the cause of the large radiance discrepancy noted. The third item is the subject of this report.

## 2. RADIOMETRIC AND SUPPORTING METEOROLOGICAL MEASUREMENTS

A liquid-nitrogen-cooled radiometer operating in the 15 $\mu$m region was flown on a balloon-borne platform launched from White Sands, New Mexico on 28 September 1977 (see Murcray, et al[4]). The intent of this measurement was to filter the radiometer in the strongest absorbing portion of the 15 $\mu$m carbon dioxide band and to view the atmosphere horizontally. Transmission calculations indicated that the atmosphere would be opaque over short horizontal distances all the way from the surface to an altitude of 20 km and that even at 30 km (the maximum height of the balloon) the atmosphere would become opaque over a horizontal distance of a few hundred kilometers. Therefore, in the lower portion of the atmosphere, the radiometer would be expected to measure the local temperature.

3. McClatchey, Robert A. (1976) Satellite Temperature Sounding of the Atmosphere: Ground Truth Analysis, AFGL-TR-76-0279, AD A038236.

4. Murcray, D.G., Murcray, F.H., Murcray, F.J., Williams, W.J. (1978) Infrared Background Measurements, AFGL-TR-78-0249, AD A062260.

At higher altitudes, a comparison between measurements and calculations could be made via the radiative transfer equation and the presumed known temperature profiles measured by rawinsonde and rocketsonde.

The liquid nitrogen used to cool the entrance aperture of the radiometer is allowed to vent out through an entrance baffle system which both cools the baffle and provides an antifrost capability for the entrance window. In order to avoid dumping liquid nitrogen, it was necessary to orient the radiometer at an elevation angle of $20^{\circ}$. This reduces somewhat the altitude at which the radiometer can be considered to be monitoring the local temperature. However, this situation can be countered by applying a radiative transfer equation at somewhat lower altitudes than originally intended. A high resolution spectrum based on the U. S. Standard Atmosphere, 1976[2] and the actual measurement geometry is given in Figure 2. This figure helps provide an understanding of the actual atmosphere opacity at float altitude.

The radiometer was carefully calibrated against a known black body on four separate occasions. No difficulties were encountered and the four calibration results were consistent to better than 0.5 percent. Consideration of other possible errors associated with calibration procedures leads to the confident statement that the radiance measurements should not be as large as 1 percent.[4]

The radiometer was filtered so that the net spectral response function of the instrument is as indicated in Figure 3. Although it was originally intended to use a narrow filter located in the Q-branch (see Figure 2) (about 1.5 $cm^{-1}$ wide centered near 668 $cm^{-1}$), it was not possible to obtain such a filter without great expense. Therefore, an available filter centered near 683 $cm^{-1}$ near the strongest portion of the R-branch was used instead. This fact also contributes to a decreased opacity at higher altitudes. This lower opacity simply requires that the measurements be analyzed by application of the radiative transfer equation at somewhat lower altitude than would otherwise be required. Figure 4 has been included to provide an indication of the net atmospheric opacity as viewed from the radiometer. It can be seen that the atmosphere becomes significantly non-opaque above 150 mb.

Figure 5 shows the details of the flight including launch time, the time the sensor was located at certain pressure altitudes, the general path of the balloon package, and the location of rawinsonde ground stations from which vertical profile information was obtained. Figure 6 shows the temperature field at the 30 mb pressure level as obtained from rawinsonde information. This figure is shown as an indication of the temperature uniformity over a broad geographical region. At this pressure altitude, the temperature can be seen to be uniform to within 1 or $2^{\circ}C$ over distances of 3000 km. Temperature data at lower altitudes show a similar degree of uniformity. This fact is important as we use the local rawinsonde

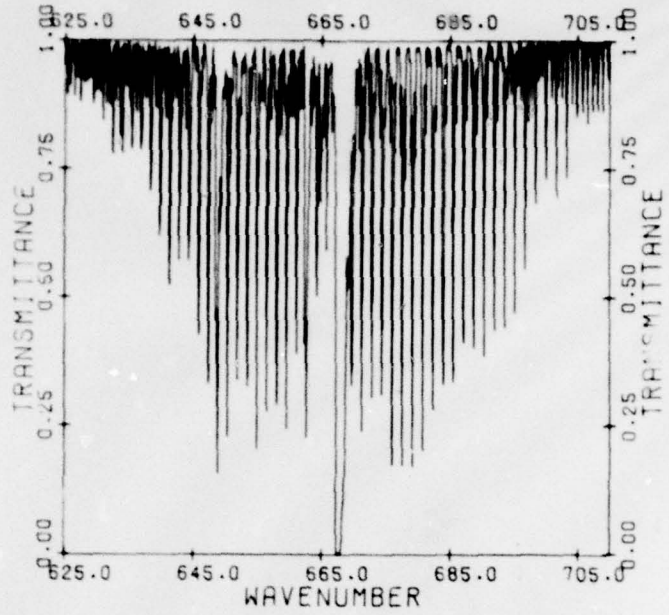


Figure 2. Calculated High Resolution Spectrum of Carbon Dioxide for a U. S. Standard Atmosphere, 1976 (Ref. 2), Looking Upward at a 20° Elevation Angle at an Altitude of 30 km

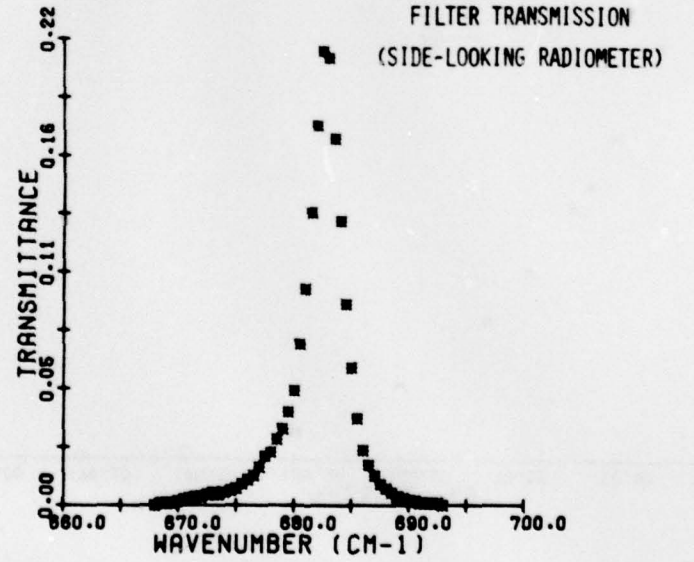


Figure 3. The Transmission Function of the Filter Used in the Side-Looking Radiometer

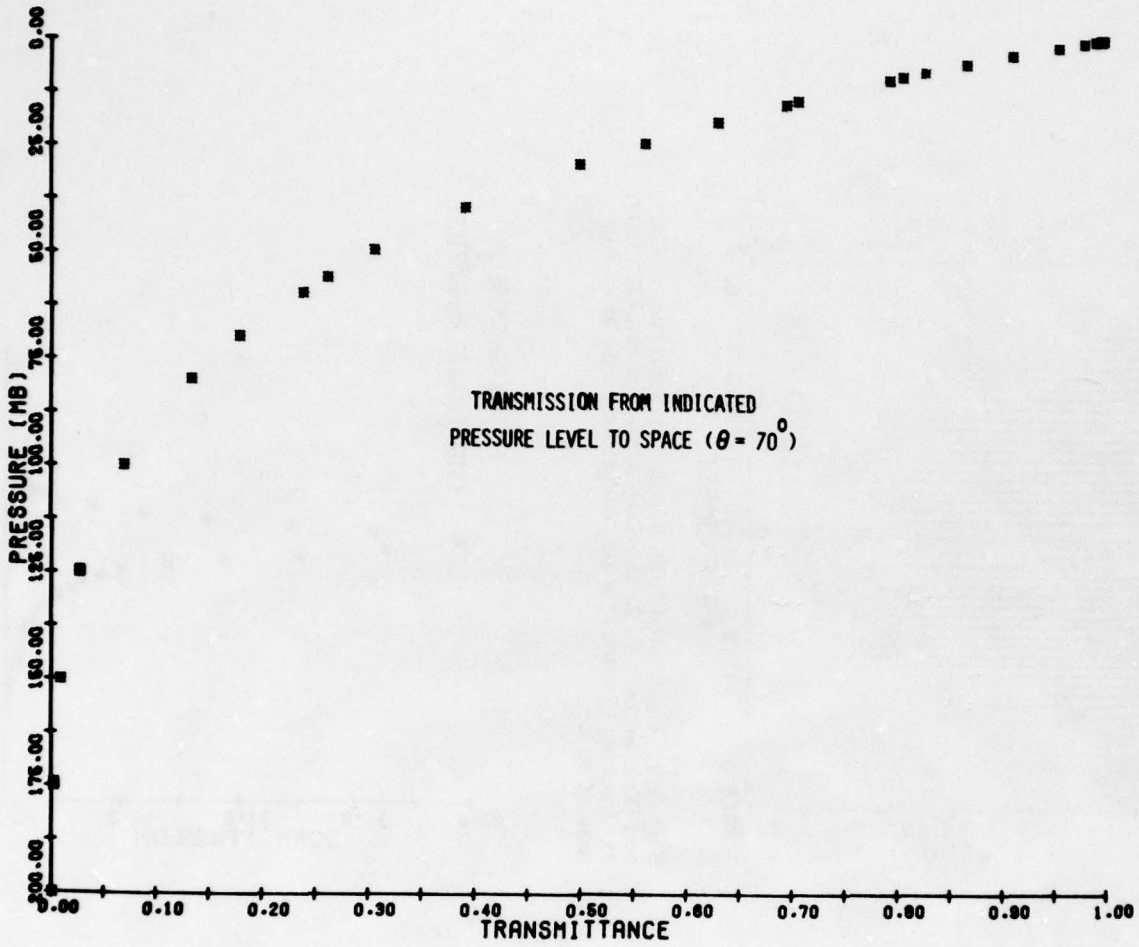


Figure 4. The Transmission From the Indicated Pressure Level to Space Along a 20° Elevation Angle (70° Zenith Angle)

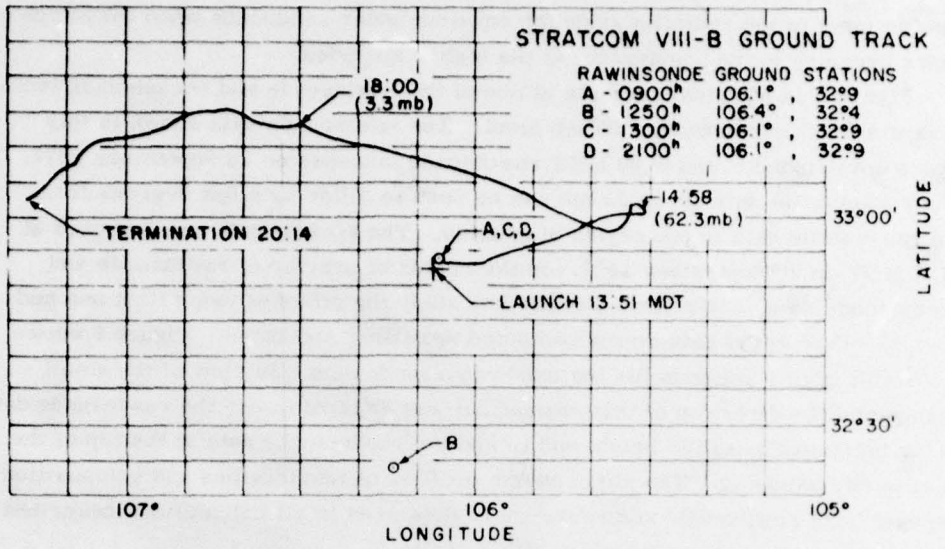


Figure 5. The Ground Track of the Balloon Payload at White Sands Missile Range, New Mexico

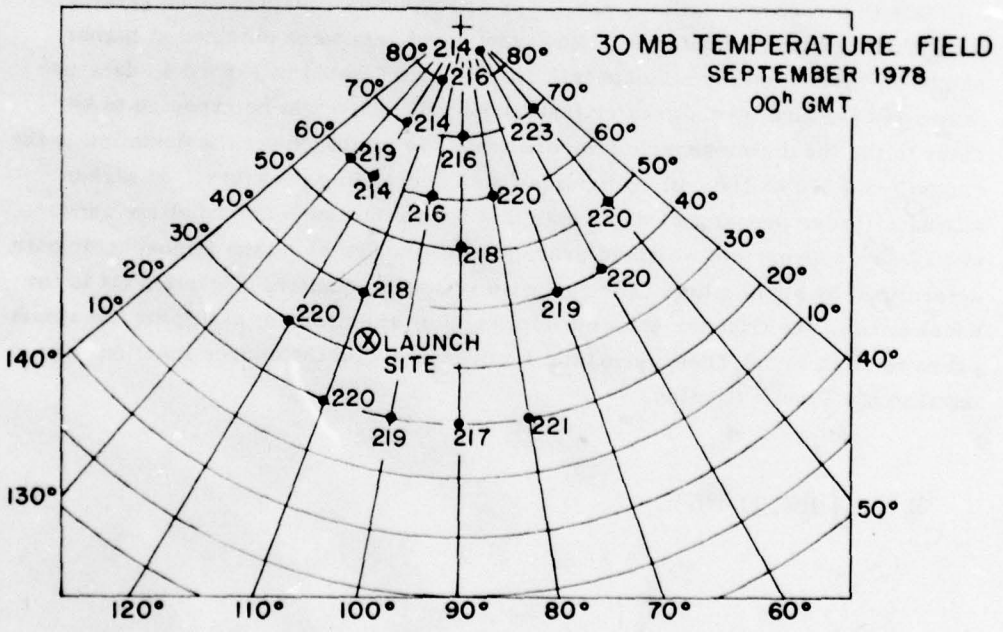


Figure 6. The 30 mb Temperature Field Over Much of the Northern Hemisphere on 28 September 1978

data as input to the radiative transfer equation under conditions when the atmosphere becomes more transparent at the higher altitudes.

Figure 7 is a typical example of one of the rawinsonde and rocketsonde temperature profiles above the 200 mb level. The rawinsonde data shown in this figure correspond to the 0900 MDT rawinsonde launched on 28 September 1977. The rocketsonde data above 25 mb can be seen to differ by a few degrees from the rawinsonde data in the region of overlap. The rocketsonde was launched at 1427 MDT on 28 September 1977. In the region of overlap of rawinsonde and rocketsonde data, some tests were run to study the effect of using first one and then the other set of data on the computed upwelling radiances. Figure 8 shows the result of this analysis for the 0900 rawinsonde data. In view of the small change and the direction of that change,* it was decided to use the rawinsonde data to the maximum possible height and to add the rocketsonde data at the top of the rawinsonde sounding. The atmospheric profiles of temperature and composition derived from rawinsonde and rocketsonde data used in all calculations described in the next section are provided in Tables 1a to 1f.

## 3. ANALYSIS OF RADIANCE MEASUREMENTS

Due to a recovery failure, the lower altitude data (for pressures greater than 290 mb) were not obtained. However, good data were obtained at higher altitudes. Based on the atmospheric opacity as indicated in Figure 4, data obtained at pressure levels greater than about 150 mb might be expected to be close to the local atmospheric temperature. We might expect the deviation in the region from 290 to 150 mb to increase with decreasing pressure. At higher altitudes (lower pressures) it is clear that the radiances received at the sensor must be an appropriate weighted average of radiances along the atmospheric path determined by application of the radiative transfer equation. Equation (1) is the usual form of the transfer equation applicable to the problem assuming the atmosphere to be in Local Thermodynamic Equilibrium with the source function set equal to the Planck function.

$$I_{\bar{\nu}} = \int B(\bar{\nu}, T)\, d\tau(\bar{\nu}) \qquad (1)$$

*(This will tend to minimize the measurement-calculation discrepancy described in Section 3.)

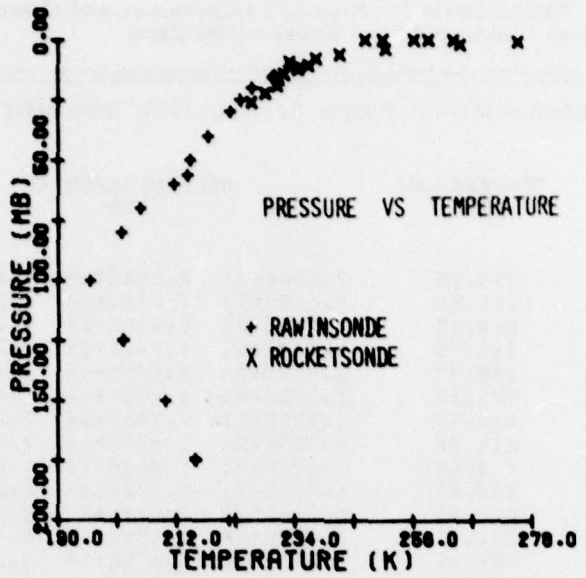


Figure 7. Typical Rawinsonde/Rocketsonde Data Obtained at 0900 MDT on 28 September 1977

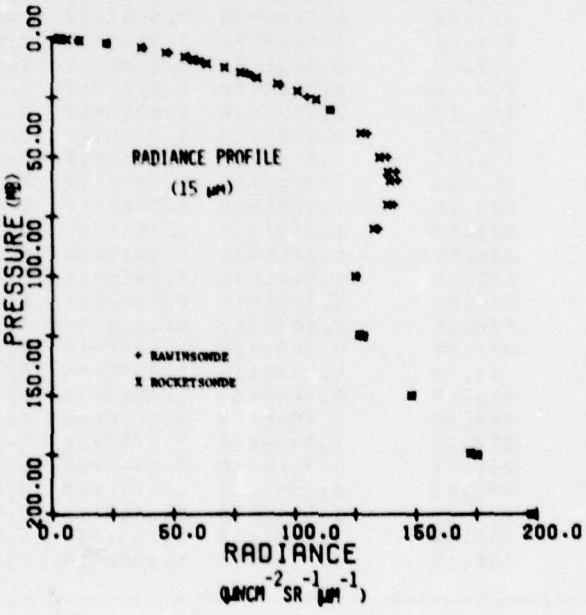


Figure 8. Radiance Profile Computed Based on Rawinsonde Data (+) and Rocketsonde Data (x) in the Region of Data Overlap as Shown in Figure 7

**Table 1a. Atmospheric Profiles of Temperature and Composition Derived from Rawinsonde and Rocketsonde Data**

White Sands Missile Range, 28 Sept. 1977, 0900 MDT

| PRESSURE (MB) | TEMPERATURE (K) | MOLECULES/SQ CM CO2 | N2O | O3 |
|---|---|---|---|---|
| 354.000 | 248.95 | 2.484E+21 | 2.108E+18 | 5.070E+17 |
| 350.000 | 248.65 | 2.450E+21 | 2.079E+18 | 5.130E+17 |
| 342.000 | 248.25 | 2.400E+21 | 2.036E+18 | 5.220E+17 |
| 300.000 | 240.35 | 2.100E+21 | 1.782E+18 | 5.767E+17 |
| 275.360 | 236.25 | 1.927E+21 | 1.635E+18 | 6.100E+17 |
| 250.000 | 231.15 | 1.750E+21 | 1.485E+18 | 6.453E+17 |
| 200.000 | 220.35 | 1.400E+21 | 1.188E+18 | 7.284E+17 |
| 177.000 | 214.85 | 1.245E+21 | 1.056E+18 | 7.579E+17 |
| 175.000 | 213.45 | 1.225E+21 | 1.040E+18 | 7.633E+17 |
| 150.000 | 207.65 | 1.050E+21 | 8.910E+17 | 8.188E+17 |
| 127.300 | 201.85 | 8.911E+20 | 7.562E+17 | 8.870E+17 |
| 125.000 | 201.65 | 8.750E+20 | 7.425E+17 | 8.958E+17 |
| 120.000 | 201.15 | 8.456E+20 | 7.176E+17 | 9.129E+17 |
| 113.000 | 198.65 | 7.966E+20 | 6.760E+17 | 9.456E+17 |
| 100.000 | 197.25 | 7.000E+20 | 5.940E+17 | 1.033E+18 |
| 89.000 | 195.65 | 6.286E+20 | 5.334E+17 | 1.121E+18 |
| 80.000 | 201.25 | 5.600E+20 | 4.752E+17 | 1.251E+18 |
| 70.000 | 207.75 | 4.900E+20 | 4.158E+17 | 1.471E+18 |
| 60.000 | 213.05 | 4.200E+20 | 3.564E+17 | 1.817E+18 |
| 56.300 | 215.25 | 3.941E+20 | 3.344E+17 | 1.975E+18 |
| 50.000 | 215.45 | 3.500E+20 | 2.970E+17 | 2.287E+18 |
| 40.000 | 217.25 | 2.800E+20 | 2.376E+17 | 2.898E+18 |
| 31.000 | 219.15 | 2.226E+20 | 1.889E+17 | 3.511E+18 |
| 30.000 | 221.65 | 2.100E+20 | 1.782E+17 | 3.668E+18 |
| 28.000 | 220.25 | 2.016E+20 | 1.711E+17 | 3.781E+18 |
| 25.000 | 221.65 | 1.750E+20 | 1.485E+17 | 4.178E+18 |
| 20.000 | 223.85 | 1.400E+20 | 1.188E+17 | 4.787E+18 |
| 19.382 | 230.75 | 1.357E+20 | 1.151E+17 | 4.869E+18 |
| 16.739 | 231.05 | 1.172E+20 | 9.943E+16 | 5.222E+18 |
| 14.463 | 232.05 | 1.012E+20 | 8.591E+16 | 5.552E+18 |
| 12.511 | 234.65 | 8.758E+19 | 7.432E+16 | 5.851E+18 |
| 10.830 | 236.55 | 7.587E+19 | 6.438E+16 | 6.116E+18 |
| 8.147 | 237.95 | 5.703E+19 | 4.839E+16 | 6.554E+18 |
| 6.157 | 242.35 | 4.310E+19 | 3.657E+16 | 6.901E+18 |
| 4.891 | 250.85 | 2.864E+19 | 2.430E+16 | 3.358E+18 |
| 2.137 | 264.65 | 1.496E+19 | 1.269E+16 | 1.128E+17 |
| 1.006 | 275.35 | 7.042E+18 | 5.976E+15 | 3.071E+16 |
| .538 | 263.45 | 3.766E+18 | 3.196E+15 | 1.479E+16 |
| .322 | 258.85 | 2.254E+18 | 1.913E+15 | 8.200E+15 |
| .203 | 256.15 | 1.581E+18 | 1.681E+15 | 7.011E+15 |
| .217 | 250.45 | 1.519E+18 | 1.289E+15 | 4.999E+15 |
| .190 | 247.15 | 1.330E+18 | 1.129E+15 | 4.175E+15 |

Table 1b. Atmospheric Profiles of Temperature and Composition Derived from Rawinsonde and Rocketsonde Data

White Sands Missile Range, 28 Sept. 1977, 1250 MDT

| PRESSURE (MB) | TEMPERATURE (K) | MOLECULES/SQ CM | | |
|---|---|---|---|---|
| | | CO2 | N2O | O3 |
| 359.000 | 250.85 | 2.519E+21 | 2.137E+18 | 5.807E+17 |
| 350.000 | 249.45 | 2.450E+21 | 2.079E+18 | 5.130E+17 |
| 300.000 | 241.35 | 2.100E+21 | 1.782E+18 | 5.767E+17 |
| 283.000 | 237.75 | 1.987E+21 | 1.686E+18 | 5.982E+17 |
| 273.000 | 236.85 | 1.917E+21 | 1.626E+18 | 6.122E+17 |
| 250.000 | 232.05 | 1.750E+21 | 1.485E+18 | 6.453E+17 |
| 200.000 | 221.85 | 1.400E+21 | 1.188E+18 | 7.204E+17 |
| 175.100 | 215.65 | 1.225E+21 | 1.040E+18 | 7.633E+17 |
| 174.300 | 215.45 | 1.220E+21 | 1.035E+18 | 7.646E+17 |
| 150.000 | 209.95 | 1.050E+21 | 8.910E+17 | 8.180E+17 |
| 125.200 | 202.15 | 8.750E+20 | 7.425E+17 | 8.958E+17 |
| 124.600 | 202.05 | 8.722E+20 | 7.401E+17 | 8.973E+17 |
| 100.000 | 195.85 | 7.000E+20 | 5.940E+17 | 1.033E+18 |
| 80.000 | 201.75 | 5.600E+20 | 4.752E+17 | 1.251E+18 |
| 70.000 | 205.35 | 4.900E+20 | 4.158E+17 | 1.471E+18 |
| 60.000 | 211.55 | 4.200E+20 | 3.564E+17 | 1.817E+18 |
| 56.300 | 214.05 | 3.941E+20 | 3.344E+17 | 1.975E+18 |
| 50.000 | 214.65 | 3.500E+20 | 2.970E+17 | 2.287E+18 |
| 40.000 | 217.85 | 2.800E+20 | 2.376E+17 | 2.898E+18 |
| 30.000 | 222.05 | 2.100E+20 | 1.782E+17 | 3.668E+18 |
| 25.000 | 223.85 | 1.750E+20 | 1.485E+17 | 4.178E+18 |
| 20.000 | 226.05 | 1.400E+20 | 1.188E+17 | 4.787E+18 |
| 15.800 | 229.95 | 1.106E+20 | 9.385E+16 | 5.353E+18 |
| 15.000 | 230.35 | 1.050E+20 | 8.910E+16 | 5.470E+18 |
| 10.000 | 233.65 | 7.000E+19 | 5.940E+16 | 6.246E+18 |
| 9.380 | 233.05 | 6.510E+19 | 5.524E+16 | 6.359E+18 |
| 8.147 | 237.95 | 5.783E+19 | 4.839E+16 | 6.554E+18 |
| 6.157 | 242.35 | 4.310E+19 | 3.657E+16 | 6.901E+18 |
| 4.091 | 250.85 | 2.864E+19 | 2.430E+16 | 3.358E+18 |
| 2.137 | 264.65 | 1.496E+19 | 1.269E+16 | 1.128E+17 |
| 1.086 | 275.35 | 7.042E+18 | 5.976E+15 | 3.071E+16 |
| .538 | 263.45 | 3.766E+18 | 3.196E+15 | 1.479E+16 |
| .322 | 258.85 | 2.254E+18 | 1.913E+15 | 8.280E+15 |
| .203 | 256.15 | 1.581E+18 | 1.681E+15 | 7.011E+15 |
| .217 | 250.45 | 1.519E+18 | 1.289E+15 | 4.999E+15 |
| .190 | 247.15 | 1.330E+18 | 1.129E+15 | 4.175E+15 |

Table 1c. Atmospheric Profiles of Temperature and Composition Derived from Rawinsonde and Rocketsonde Data

White Sands Missile Range, 28 Sept. 1977, 1300 MDT

| PRESSURE (MB) | TEMPERATURE (K) | MOLECULES/SQ CM CO2 | N2O | O3 |
|---|---|---|---|---|
| 382.000 | 253.25 | 2.688E+21 | 2.274E+18 | 4.722E+17 |
| 363.000 | 251.45 | 2.547E+21 | 2.161E+18 | 4.957E+17 |
| 350.000 | 249.45 | 2.458E+21 | 2.079E+18 | 5.138E+17 |
| 300.000 | 241.45 | 2.108E+21 | 1.782E+18 | 5.787E+17 |
| 260.000 | 236.55 | 1.802E+21 | 1.597E+18 | 6.193E+17 |
| 250.000 | 232.55 | 1.758E+21 | 1.485E+18 | 6.453E+17 |
| 240.000 | 228.75 | 1.688E+21 | 1.188E+18 | 7.284E+17 |
| 175.000 | 214.05 | 1.225E+21 | 1.048E+18 | 7.683E+17 |
| 173.000 | 213.75 | 1.217E+21 | 1.032E+18 | 7.696E+17 |
| 150.000 | 208.65 | 1.050E+21 | 8.910E+17 | 8.188E+17 |
| 125.000 | 201.85 | 8.758E+20 | 7.425E+17 | 8.958E+17 |
| 124.000 | 201.75 | 8.736E+20 | 7.413E+17 | 8.965E+17 |
| 105.000 | 198.25 | 7.406E+20 | 6.285E+17 | 9.527E+17 |
| 100.000 | 198.55 | 7.088E+20 | 5.940E+17 | 1.033E+18 |
| 91.000 | 197.45 | 6.378E+20 | 5.405E+17 | 1.118E+18 |
| 80.000 | 201.75 | 5.688E+20 | 4.752E+17 | 1.291E+18 |
| 70.000 | 206.25 | 4.988E+20 | 4.158E+17 | 1.471E+18 |
| 60.000 | 211.55 | 4.208E+20 | 3.564E+17 | 1.817E+18 |
| 54.000 | 214.65 | 3.836E+20 | 3.255E+17 | 2.042E+18 |
| 50.000 | 215.15 | 3.588E+20 | 2.970E+17 | 2.287E+18 |
| 40.000 | 216.85 | 2.888E+20 | 2.376E+17 | 2.898E+18 |
| 30.000 | 221.75 | 2.188E+20 | 1.782E+17 | 3.668E+18 |
| 25.300 | 225.65 | 1.771E+20 | 1.503E+17 | 4.144E+18 |
| 25.000 | 225.75 | 1.758E+20 | 1.485E+17 | 4.178E+18 |
| 20.000 | 227.05 | 1.488E+20 | 1.188E+17 | 4.787E+18 |
| 15.000 | 229.85 | 1.058E+20 | 8.910E+16 | 5.478E+18 |
| 11.000 | 232.15 | 8.260E+19 | 7.089E+16 | 5.963E+18 |
| 10.038 | 236.55 | 7.587E+19 | 6.438E+16 | 6.116E+18 |
| 6.147 | 237.95 | 5.703E+19 | 4.839E+16 | 6.554E+18 |
| 6.157 | 242.35 | 4.318E+19 | 3.697E+16 | 6.981E+18 |
| 4.091 | 256.85 | 2.864E+19 | 2.438E+16 | 8.358E+18 |
| 2.137 | 264.85 | 1.496E+19 | 1.269E+16 | 1.128E+17 |
| 1.006 | 275.35 | 7.042E+18 | 5.976E+15 | 3.071E+16 |
| .538 | 263.45 | 3.766E+18 | 3.196E+15 | 1.479E+16 |
| .322 | 250.85 | 2.254E+18 | 1.913E+15 | 8.288E+15 |
| .203 | 256.15 | 1.581E+18 | 1.821E+15 | 7.811E+15 |
| .217 | 250.45 | 1.519E+18 | 1.289E+15 | 4.999E+15 |
| .190 | 247.15 | 1.338E+18 | 1.129E+15 | 4.175E+15 |

Table 1d. Atmospheric Profiles of Temperature and Composition Derived from Rawinsonde and Rocketsonde Data

White Sands Missile Range, 28 Sept. 1977, 2100 MDT

| PRESSURE (MB) | TEMPERATURE (K) | MOLECULES/SQ CM CO2 | N2O | O3 |
|---|---|---|---|---|
| 361.000 | 249.45 | 2.527E+21 | 2.144E+18 | 4.992E+17 |
| 355.000 | 249.45 | 2.491E+21 | 2.113E+18 | 5.057E+17 |
| 348.000 | 239.65 | 2.108E+21 | 1.782E+18 | 5.767E+17 |
| 292.300 | 230.25 | 2.046E+21 | 1.736E+18 | 5.866E+17 |
| 282.300 | 237.25 | 1.976E+21 | 1.677E+18 | 6.082E+17 |
| 250.000 | 231.85 | 1.758E+21 | 1.485E+18 | 6.453E+17 |
| 231.000 | 227.65 | 1.623E+21 | 1.377E+18 | 6.712E+17 |
| 200.000 | 220.75 | 1.408E+21 | 1.188E+18 | 7.204E+17 |
| 183.300 | 215.95 | 1.283E+21 | 1.089E+18 | 7.482E+17 |
| 150.000 | 207.45 | 1.050E+21 | 8.910E+17 | 8.180E+17 |
| 136.300 | 204.15 | 9.541E+20 | 8.096E+17 | 8.564E+17 |
| 120.300 | 201.65 | 8.421E+20 | 7.146E+17 | 9.152E+17 |
| 117.300 | 204.15 | 8.211E+20 | 6.968E+17 | 9.291E+17 |
| 100.000 | 200.25 | 7.000E+20 | 5.940E+17 | 1.033E+18 |
| 95.300 | 197.75 | 6.671E+20 | 5.661E+17 | 1.071E+18 |
| 83.300 | 199.35 | 5.831E+20 | 4.948E+17 | 1.181E+18 |
| 70.000 | 206.95 | 4.900E+20 | 4.158E+17 | 1.471E+18 |
| 58.000 | 215.95 | 3.500E+20 | 2.970E+17 | 2.287E+18 |
| 30.300 | 216.25 | 2.681E+20 | 2.275E+17 | 3.017E+18 |
| 30.000 | 220.05 | 2.100E+20 | 1.782E+17 | 3.668E+18 |
| 20.000 | 226.25 | 1.400E+20 | 1.188E+17 | 4.787E+18 |
| 14.300 | 226.05 | 1.001E+20 | 8.494E+16 | 5.577E+18 |
| 12.500 | 227.35 | 8.750E+19 | 7.425E+16 | 5.852E+18 |
| 10.030 | 236.95 | 7.507E+19 | 6.438E+16 | 6.116E+18 |
| 8.147 | 237.95 | 5.703E+19 | 4.839E+16 | 6.554E+18 |
| 6.157 | 242.35 | 4.310E+19 | 3.657E+16 | 6.981E+18 |
| 4.091 | 250.05 | 2.864E+19 | 2.430E+16 | 3.358E+18 |
| 2.137 | 264.65 | 1.496E+19 | 1.269E+16 | 1.128E+17 |
| 1.006 | 275.35 | 7.042E+18 | 5.976E+15 | 3.071E+16 |
| .538 | 263.45 | 3.766E+18 | 3.196E+15 | 1.479E+16 |
| .322 | 258.85 | 2.254E+18 | 1.913E+15 | 8.280E+15 |
| .283 | 256.15 | 1.981E+18 | 1.681E+15 | 7.011E+15 |
| .217 | 250.45 | 1.519E+18 | 1.289E+15 | 4.999E+15 |
| .190 | 247.15 | 1.330E+18 | 1.129E+15 | 4.175E+15 |

Table 1e. Atmospheric Profiles of Temperature and Composition Derived from Rawinsonde and Rocketsonde Data

EL PASO, TX

| PRESSURE (MB) | TEMPERATURE (K) | MOLECULES/SQ CM | | |
|---|---|---|---|---|
| | | CO2 | N2O | O3 |
| 350.000 | 247.95 | 2.450E+21 | 2.079E+18 | 5.130E+17 |
| 300.000 | 239.85 | 2.100E+21 | 1.782E+18 | 5.767E+17 |
| 250.000 | 229.35 | 1.750E+21 | 1.485E+18 | 6.453E+17 |
| 200.000 | 219.65 | 1.400E+21 | 1.188E+18 | 7.204E+17 |
| 170.000 | 211.85 | 1.190E+21 | 1.010E+18 | 7.728E+17 |
| 145.000 | 203.95 | 1.015E+21 | 8.613E+17 | 8.313E+17 |
| 130.000 | 200.85 | 9.100E+20 | 7.722E+17 | 8.771E+17 |
| 100.000 | 194.85 | 7.000E+20 | 5.940E+17 | 1.033E+18 |
| 95.000 | 196.65 | 6.650E+20 | 5.643E+17 | 1.074E+18 |
| 90.000 | 198.45 | 6.300E+20 | 5.346E+17 | 1.119E+18 |
| 85.000 | 200.65 | 5.950E+20 | 5.049E+17 | 1.177E+18 |
| 80.000 | 203.05 | 5.600E+20 | 4.752E+17 | 1.251E+18 |
| 75.000 | 205.15 | 5.250E+20 | 4.455E+17 | 1.352E+18 |
| 70.000 | 207.35 | 4.900E+20 | 4.158E+17 | 1.471E+18 |
| 65.000 | 209.25 | 4.550E+20 | 3.861E+17 | 1.626E+18 |
| 60.000 | 211.35 | 4.200E+20 | 3.564E+17 | 1.817E+18 |
| 55.000 | 213.65 | 3.850E+20 | 3.267E+17 | 2.032E+18 |
| 50.000 | 215.95 | 3.500E+20 | 2.970E+17 | 2.287E+18 |
| 45.000 | 216.25 | 3.150E+20 | 2.673E+17 | 2.575E+18 |
| 40.000 | 216.85 | 2.800E+20 | 2.376E+17 | 2.898E+18 |
| 36.000 | 217.35 | 2.520E+20 | 2.138E+17 | 3.182E+18 |
| 33.000 | 217.95 | 2.310E+20 | 1.960E+17 | 3.411E+18 |
| 30.000 | 218.05 | 2.100E+20 | 1.782E+17 | 3.668E+18 |
| 26.000 | 220.25 | 1.820E+20 | 1.544E+17 | 4.067E+18 |
| 23.000 | 222.15 | 1.610E+20 | 1.366E+17 | 4.412E+18 |
| 20.000 | 223.65 | 1.400E+20 | 1.188E+17 | 4.787E+18 |
| 18.000 | 225.65 | 1.260E+20 | 1.069E+17 | 5.052E+18 |
| 16.000 | 228.15 | 1.120E+20 | 9.504E+16 | 5.324E+18 |
| 14.300 | 230.15 | 1.001E+20 | 8.494E+16 | 5.577E+18 |
| 12.000 | 230.25 | 8.400E+19 | 7.128E+16 | 5.931E+18 |
| 10.000 | 230.35 | 7.000E+19 | 5.940E+16 | 6.246E+18 |
| 8.147 | 237.95 | 5.703E+19 | 4.839E+16 | 6.554E+18 |
| 6.157 | 242.35 | 4.310E+19 | 3.657E+16 | 6.901E+18 |
| 4.091 | 250.85 | 2.864E+19 | 2.430E+16 | 3.358E+18 |
| 2.137 | 264.65 | 1.496E+19 | 1.269E+16 | 1.128E+17 |
| 1.006 | 275.35 | 7.042E+18 | 5.976E+15 | 3.071E+16 |
| .538 | 263.45 | 3.766E+18 | 3.196E+15 | 1.479E+16 |
| .322 | 258.85 | 2.254E+18 | 1.913E+15 | 8.200E+15 |
| .283 | 256.15 | 1.981E+18 | 1.681E+15 | 7.011E+15 |
| .217 | 250.45 | 1.519E+18 | 1.289E+15 | 4.959E+15 |
| .190 | 247.15 | 1.330E+18 | 1.129E+15 | 4.179E+15 |

Table 1f. Atmospheric Profiles of Temperature and Composition Derived from Rawinsonde and Rocketsonde Data

ALBUQUERQUE, NM

| PRESSURE (MB) | TEMPERATURE (K) | MOLECULES/SQ CM | | |
|---|---|---|---|---|
| | | CO2 | N2O | O3 |
| 350.000 | 245.05 | 2.450E+21 | 2.079E+18 | 9.130E+17 |
| 300.000 | 238.45 | 2.100E+21 | 1.782E+18 | 8.767E+17 |
| 250.000 | 229.95 | 1.750E+21 | 1.485E+18 | 8.453E+17 |
| 200.000 | 221.15 | 1.400E+21 | 1.188E+18 | 7.206E+17 |
| 175.000 | 214.35 | 1.225E+21 | 1.040E+18 | 7.633E+17 |
| 150.000 | 207.85 | 1.050E+21 | 8.910E+17 | 8.188E+17 |
| 122.000 | 200.25 | 8.540E+20 | 7.247E+17 | 9.073E+17 |
| 100.000 | 200.15 | 7.000E+20 | 5.940E+17 | 1.033E+18 |
| 92.500 | 198.15 | 6.475E+20 | 5.495E+17 | 1.097E+18 |
| 88.500 | 202.05 | 6.195E+20 | 5.257E+17 | 1.136E+18 |
| 83.500 | 200.05 | 5.845E+20 | 4.960E+17 | 1.198E+18 |
| 80.000 | 201.15 | 5.600E+20 | 4.752E+17 | 1.251E+18 |
| 75.000 | 204.35 | 5.250E+20 | 4.455E+17 | 1.352E+18 |
| 70.000 | 207.25 | 4.900E+20 | 4.158E+17 | 1.471E+18 |
| 65.000 | 210.25 | 4.550E+20 | 3.861E+17 | 1.626E+18 |
| 61.500 | 213.15 | 4.305E+20 | 3.653E+17 | 1.758E+18 |
| 60.000 | 213.25 | 4.200E+20 | 3.564E+17 | 1.817E+18 |
| 55.000 | 213.95 | 3.850E+20 | 3.267E+17 | 2.032E+18 |
| 50.000 | 214.25 | 3.500E+20 | 2.970E+17 | 2.287E+18 |
| 45.000 | 215.95 | 3.150E+20 | 2.673E+17 | 2.575E+18 |
| 40.000 | 218.35 | 2.800E+20 | 2.376E+17 | 2.898E+18 |
| 36.500 | 218.95 | 2.555E+20 | 2.168E+17 | 3.145E+18 |
| 32.300 | 217.15 | 2.261E+20 | 1.919E+17 | 3.469E+18 |
| 30.000 | 220.65 | 2.100E+20 | 1.782E+17 | 3.668E+18 |
| 26.000 | 222.25 | 1.820E+20 | 1.544E+17 | 4.067E+18 |
| 23.000 | 223.65 | 1.610E+20 | 1.366E+17 | 4.412E+18 |
| 20.000 | 225.35 | 1.400E+20 | 1.188E+17 | 4.787E+18 |
| 18.000 | 226.95 | 1.260E+20 | 1.069E+17 | 5.052E+18 |
| 16.000 | 228.85 | 1.120E+20 | 9.504E+16 | 5.324E+18 |
| 14.300 | 230.85 | 1.001E+20 | 8.494E+16 | 5.577E+18 |
| 12.000 | 230.85 | 8.400E+19 | 7.128E+16 | 5.931E+18 |
| 10.000 | 230.85 | 7.000E+19 | 5.940E+16 | 6.246E+18 |
| 8.147 | 237.95 | 5.703E+19 | 4.839E+16 | 6.554E+18 |
| 6.157 | 242.35 | 4.310E+19 | 3.657E+16 | 6.981E+18 |
| 4.091 | 250.85 | 2.864E+19 | 2.430E+16 | 8.358E+18 |
| 2.137 | 264.65 | 1.496E+19 | 1.269E+16 | 1.128E+17 |
| 1.006 | 275.35 | 7.042E+18 | 5.976E+15 | 3.071E+16 |
| .538 | 263.45 | 3.766E+18 | 3.196E+15 | 1.479E+16 |
| .322 | 258.85 | 2.254E+18 | 1.913E+15 | 8.208E+15 |
| .283 | 256.15 | 1.981E+18 | 1.681E+15 | 7.811E+15 |
| .217 | 250.45 | 1.519E+18 | 1.289E+15 | 4.999E+15 |
| .190 | 247.15 | 1.330E+18 | 1.129E+15 | 4.175E+15 |

where

$I_{\bar{\nu}}$ is the radiance received at the sensor;

$\bar{\nu}$ is the mean frequency of the filter;

$B(\bar{\nu}, T)$ is the Planck Function associated with frequency $\bar{\nu}$ and temperature T;

$\tau(\bar{\nu})$ is the transmittance from points in the atmosphere (where the temperature is T) to the point of observation. This transmittance is a weighted average over the filter function shown in Figure 3.

Initially, the four rawinsonde data sets obtained at White Sands, New Mexico were used directly in a numerical analogue of Eq. (1). The transmission results were computed with the AFGL Atmospheric Absorption Line Parameters Compilation and a line-by-line calculation scheme similar to the one described by McClatchey et al[5] but applied to a multi-layered atmosphere was used. The transmission results were calculated in this way from each pressure level specified in the rawinsonde data of Table 1 to each lower pressure level in the same sounding along a $20^{\circ}$ elevation angle.

It was felt that the irregular spacing of the rawinsonde pressure levels might lead to computational errors. This could be a particular problem if large intervals occur at altitudes where the transmission changes rapidly from near unity to near zero. In order to avoid this problem and reduce the risk of a substantial computational uncertainty, it was decided to define a much finer pressure mesh and then to interpolate the transmission and temperature values associated with an individual rawinsonde run to this revised pressure mesh.

Under the assumption that processes in the atmosphere are adiabatic (a reasonable assumption in the bulk of the troposphere), the relation expressed as Eq. (2) can be derived (see Gordon[6]) where $\kappa$ is the ratio of the universal gas constant to the specific heat of dry air at constant pressure.

$$T = \text{Const.} \times P^{\kappa} \qquad (2)$$

The value of $\kappa$ is $0.286 \approx 2/7$. To the extent that this relation is valid, it can be seen that equal increments of $p^{2/7}$ would yield equal temperature increments. An examination of the hydrostatic equation indicates that equal height increments will

---

5. McClatchey, R.A., Benedict, W.S., Clough, S.A., Burch, D.E., Calfee, R.F., Fox, K., Rothman, L.S., Garing, J.S. (1973) The AFCRL Atmospheric Absorption Line Parameters Compilation, AFCRL-TR-73-0096, AD 762904.

6. Gordon, A.H. (1962) Elements of Dynamic Meteorology, D. Van Nostrand Co., Inc., Princeton, N.J.

also result. As temperature is one of the important atmospheric parameters governing the emitted radiance, we have chosen equal increments of $p^{2/7}$ as the basis of increasing the number of atmospheric levels for computational purposes. In this way we have increased the number of levels from a typical rawinsonde set of about 40 to 100 levels.

Having extended the independent variable array as indicated above, the following interpolation procedures were devised for the transmission and temperature respectively; 1) The transmission computed at the initial rawinsonde levels was interpolated exponentially with pressure; and 2) The temperature interpolation was carried out on the basis of Eq. (2), but with the exponent determined from the pressure and temperature values in adjacent rawinsonde levels. Test results were computed with the atmosphere above the 350 mb level divided into 100 and 200 levels and the results compared with those based on the original rawinsonde set of about 40. Changes of a few percent occurred when the 100-level results were compared with the 40-level results. The further increase to 200-levels caused a negligible further change in the resulting radiances. Therefore, all remaining calculations were performed with 100-level atmospheric models.

Figures 9a and 9b provide a composite of the calculated radiances based on the four White Sands data sets and the direct comparison of calculations with measurements. We have plotted the radiances based on the "local temperature" (assuming that the Planck function, $B(\bar{\nu}, T)$ associated with the local temperature represents the total radiance). This will be the case if the atmosphere becomes opaque in a depth over which the temperature does not change from the local value. We have also applied Eq. (1) to the calculation of radiance based on the rawinsonde/rocketsonde profiles obtained at each of the indicated times. Although the measured radiances are seen to agree rather well with the "local temperature" radiance values in the range from 290-150 mb, it can be seen that there is a clear systematic discrepancy between the measurements and the (presumably more accurate) radiative transfer calculations (symbols in Figures 9a and 9b). The "local temperature" results clearly fail for pressures less than 125 mb, but we would assume our radiative transfer calculations to represent the measured radiances rather well. The disagreement between measured and calculated radiances is seen to increase to a maximum value near 50 mb of about 20 percent. It is interesting to note that the general shape of the calculated and measured radiances match even though their absolute values do not. It should also be noted that the spread in calculated radiance values associated with these four different atmospheric profiles (see Table 1a to 1f), is small. Thus, it seems unlikely that some local temperature anomaly associated with the radiometer flight path is the cause of this discrepancy.

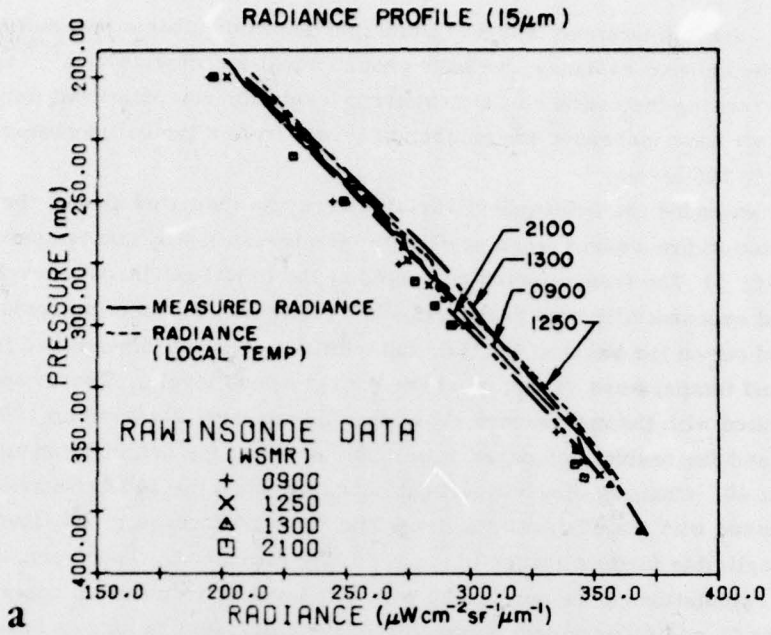


a

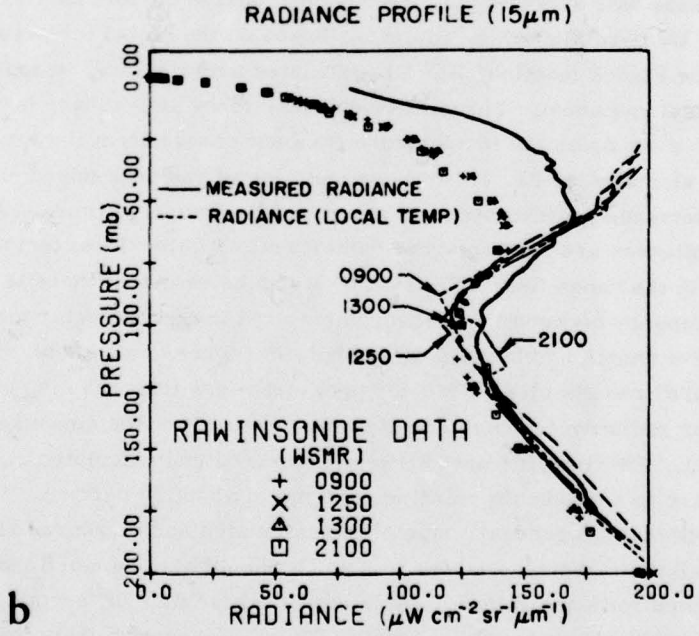


b

**Figure 9. Computed vs Measured Radiance Profiles. Computed points are the results of application of the radiative transfer equation. Computed curves result from the equivalent radiances derived from local temperature values. Results are provided for the four different White Sands Missile Range rawinsonde data sets**

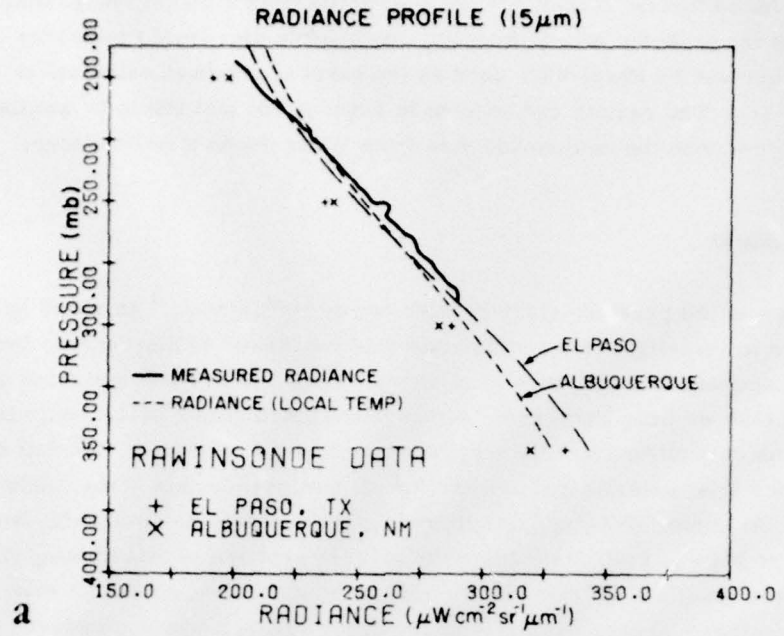


a

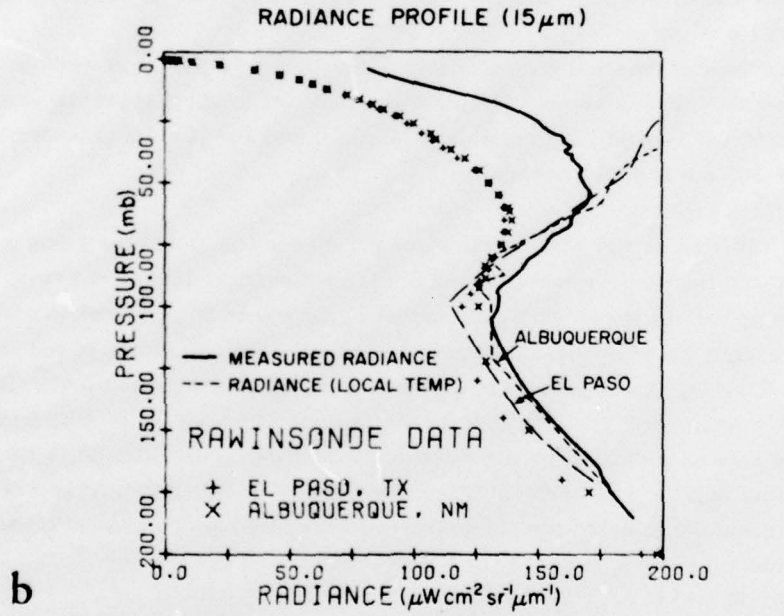


b

**Figure 10.** Computed vs Measured Radiance Profiles. Computed points are the result of application of the radiative transfer equation. Computed curves result from the equivalent radiances derived from local temperature values. Results are provided for the Albuquerque and El Paso rawinsonde data sets

In order to further investigate the possibility of this discrepancy being related to an atmospheric non-uniformity, rawinsonde data from two nearby stations (Albuquerque and El Paso) were used as the basis of radiance calculations again using Eq. (1). The results can be seen in Figures 10a and 10b to be similar to those obtained with the rawinsonde data from White Sands Missile Range.

## 4. CONCLUSIONS

In view of the previous study carried out by McClatchey,[3] an effort has been made here to investigate a possible source of the identified discrepancy between computed and satellite-measured radiances. We seem to have generated more questions than we have answered. Although the calculations in the range from 290-150 mb only differ from the measurements by a few percent, the fact that the discrepancy is systematic and similar for all rawinsonde data gives cause for concern. At higher altitudes, this discrepancy increases to intolerable levels. How can we hope to adequately solve the inverse problem of determining the temperature profile from radiometric measurements when we cannot even match our calculations and measurements under conditions of a well documented atmosphere, well-calibrated instrumentation, and carefully constructed computation techniques?

Let us look at the implication of this discrepancy as though it were attributed to transmission errors alone. For this purpose, we might inspect the results in the two different regimes indicated on Figures 9 and 10. Let us consider separately the 250 mb and 50 mb results:

i) At 250 mb

In view of the general agreement between the "local temperature" radiances and the measured radiances in the region from 290 mb-150 mb, it is clear that an extremely large transmission error would be required to explain the discrepancy between measured radiances and those calculated based on Eq. (1). That is, the atmospheric distance over which the transmission falls from 1.0 to near zero would have to be represented by a uniform temperature. The lapse rate as indicated by the rawinsonde profiles (see Table 1) is rather steep in this region. An error of 50 to 100 percent in calculated transmission would be required to drive the computed radiances into agreement with the measurements.

ii) At 50 mb

The measured radiance is about 167 $\mu w/cm^2$ sr $\mu m$ compared with a calculated value of 137.4 $\mu w/cm^2$ sr $\mu m$. Our calculations clearly show that the transmission to space along a path at a $20^o$ elevation angle should be 0.31. In other words, at this altitude and for the path of observation, the atmosphere is

clearly not opaque. Let us estimate the net transmission modification required for the calculation to agree with the measurement. To do this, we assume that we can define a mean Planck radiance for the entire path from sensor to space. We would have (from Eq. (1)), $I(\overline{\nu}) = B(\overline{\nu}, T)(1 - \tau(\overline{\nu}))$, with $I(\overline{\nu}) = 137.4$ and $\tau(\overline{\nu}) = 0.31$. Thus, the mean Planck radiance is 199.1. The radiance discrepancy would imply that the transmission satisfy the equation, $167 = 199.13\ (1 - \tau(\overline{\nu}))$. The resulting transmission would be 0.16, a factor of 2 lower than the calculated value. A careful analysis of our transmission calculation accuracy is being conducted, and at the moment, we feel that this kind of error is far outside the range of possible transmission uncertainty.

In both the 250 mb and the 50 mb measurements, the results indicate that the atmosphere is apparently more opaque than we calculate. An alternative description is that our calculation underestimates the near field radiances. These results could also be explained by atmospheric temperatures which are, in fact, higher than we think. It could also result from some additional source of atmospheric radiation.

It is useful to compare the results obtained from these in-situ measurements with the earlier study of satellite-observed radiances. At first glance, the results might appear to oppose each other, the satellite study yielding a positive calculation-measurement discrepancy and the current study yielding a negative calculation-measurement result. However, a common thread can be found. The satellite discrepancy occurs primarily in the wing of the carbon dioxide band where the satellite sensor channels sound the troposphere. An effect which manifests itself as an apparent increase in atmospheric opacity over our calculations would tend toward observing the atmosphere at higher altitude where temperatures (and emitted radiances) are less. Both these discrepant results are compatible with the interpretation that the calculations underestimate the near field contributing to the radiance and conversely overestimate the radiance from the far field.

In summary, we feel that the radiance discrepancies described in this report are real. They are consistent with the results described earlier (Ref. 3) in connection with the DMSP satellite radiances. Furthermore, we feel that the discrepancies cannot be attributed to the more obvious effects of instrument calibration, atmospheric transmission, or lack of atmospheric temperature uniformity. An examination of Eq. (1) leads us to the conclusion that the only remaining source of error may be the assumption that the source function is equal to the Planck intensity. This possibility has sufficiently large ramifications to remote sounding that we feel it should be investigated further.

We intend to pursue this problem further with the launch of two radiometers (one operating in the 15 $\mu$m and one in the 4.3 $\mu$m $CO_2$ bands) as part of a balloon flight payload. We are hopeful to make measurements starting at lower altitudes

and to reduce the elevation angle of those measurements. Furthermore the increased opacity of the 4.3 $\mu$m $CO_2$ band increases the altitude at which our radiometer can be used to measure the local atmospheric temperature.

## References


1. Kaplan, L. D. (1959) Inference of atmospheric structure from remote radiation measurements, J. Op. Soc. Amer. 49:1004.

2. U. S. Standard Atmosphere (1976) NOAA-S/T 76-1562, Supt. of Documents, U. S. Government Printing Office.

3. McClatchey, Robert A. (1976) Satellite Temperature Sounding of the Atmosphere: Ground Truth Analysis, AFGL-TR-76-0279, AD A038236.

4. Murcray, D. G., Murcray, F. H., Murcray, F. J., Williams, W. J. (1978) Infrared Background Measurements, AFGL-TR-78-0249, AD A062260.

5. McClatchey, R. A., Benedict, W. S., Clough, S. A., Burch, D. E., Calfee, R. F., Fox, K., Rothman, L. S., Garing, J. S. (1973) The AFCRL Atmospheric Absorption Line Parameters Compilation, AFCRL-TR-73-0096, AD 762904.

6. Gordon, A. H. (1962) Elements of Dynamic Meteorology, D. Van Nostrand Co., Inc., Princeton, N.J.